ACS Sustainable Chemistry & Engineering

pubs.acs.org/journal/ascecg

Research Article

Electrocatalytic Membranes for Tunable Syngas Production and High-Efficiency Delivery to Biocompatible Electrolytes

Xiaobo Zhu, Joshua Jack, Yanhong Bian, Xi Chen, Nicolas Tsesmetzis, and Zhiyong Jason Ren*

Cite This: *ACS Sustainable Chem. Eng.* 2021, 9, 6012–6022

Read Online

ACCESS | Metrics & More | Article Recommendations | Supporting Information

ABSTRACT: The integration of electrochemical and biological CO_2 reduction in artificial photosynthetic processes holds great promise to alleviate the current environmental stress of carbon-intensive industries and enable a circular carbon economy. The advancement of these devices hinges on the development of highly stable and selective CO_2 reduction catalysts that can operate in an array of biocompatible conditions. Here, we fabricated a porous silver gas diffusion electrode (GDE) on the carbon nanotube (CNT)-supported hydrophobic membrane for tunable electrochemical syngas production. We then tested its performance under the direct gas delivery mode, different chamber thicknesses, and different microbial−electrolyte compositions. Distinct from traditional flow-by delivery, CO_2 was directly flowed through the GDE and electrochemically converted to syngas and delivered into the electrolyte. The optimized reactor with the narrower chamber enabled higher CO faradic efficiencies (FEs) (~92 vs ~42%) and larger tunable CO/H_2 ratios (35:65 to 91:9 vs 12:88 to 41:59). The impact of complex microbial growth media on electrocatalysis was also investigated, and it was found that the systems achieved consistent >90% FE for syngas production, but nutrient ingredients such as NH_4Cl and yeast extract led to much higher H_2 production due to the significant increase in proton availability from these species. The culmination of these findings helps address key limitations at the microbial−electrode interface that aid in the development of practical artificial photosynthetic technologies toward the sustainable production of green fuels and chemicals.

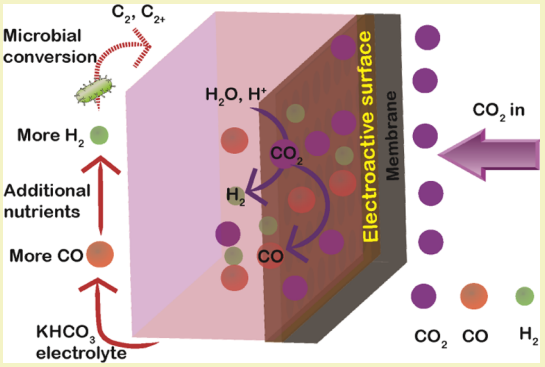

KEYWORDS: *electroactive membrane, CO_2 electrolysis, tunable syngas, biocompatible*

INTRODUCTION

Anthropogenic CO_2 emissions disrupts the natural carbon cycle, leading to rising global temperatures and increased occurrences of extreme weather events.[1,2] Carbon capture, storage, and utilization have been implemented to mitigate the impacts of such emissions while in the meantime utilizing CO_2 as a potential feedstock for beneficial reuse.[3−6] Waste CO_2 can be converted to value-added products using electro-, photo-, and biocatalytic pathways, and a wide range of products ranging from synthesis gas to organic carbonates, carboxylic acids, and alcohols have been generated to balance the carbon cycle and replace fuels and chemicals currently produced from fossil fuel sources.[4]

Electrochemical CO_2 reduction reaction (CO_2RR) carries a distinct advantage to utilize the increasingly abundant and low-cost renewable electricity for carbon recycling.[5,6] In a CO_2 electrolyzer, catalytic components (e.g., metals, carbon-based materials, and molecular catalysts) on the electrode surface convert adsorbed CO_2 into chemical products under applied electrochemical potentials.[7−11] To date, large environmental impact and high selectivity have been demonstrated for C1−C2 carbon products (e.g., CO, formate, ethylene, ethanol).[5] For example, electrochemical CO_2 reduction to syngas is a technologically favored process and brings a large environmental benefit. Recent life cycle assessment identified syngas as one of the most promising products with a substantial CO_2 reduction.[12] Assuming all global syngas production volume (150 Mtonne) is generated from the electrochemical process coupled with renewable electricity, this would lead to an annual CO_2 reduction of 12 Mtonne when comparing to the existing industrial process of steam methane reforming and coal gasification. Additionally, this electrochemical syngas generation route could reduce 39 Mtonne CO_2 emission with respect to the thermochemical CO_2 conversion route. The state of electrochemical CO_2 reduction to CO can reach up to >90% faradic efficiency (FE), and partial current density of 5−20 mA/cm^2 (at 0.4−0.6 V vs reversible hydrogen electrode (RHE)), which is equivalent to 549−2195 L-CO/(m^2 day).[5] However, these shorter chain carbons have low

Received: February 18, 2021
Revised: March 30, 2021
Published: April 21, 2021

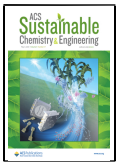

https://doi.org/10.1021/acssuschemeng.1c01150
ACS Sustainable Chem. Eng. 2021, 9, 6012−6022

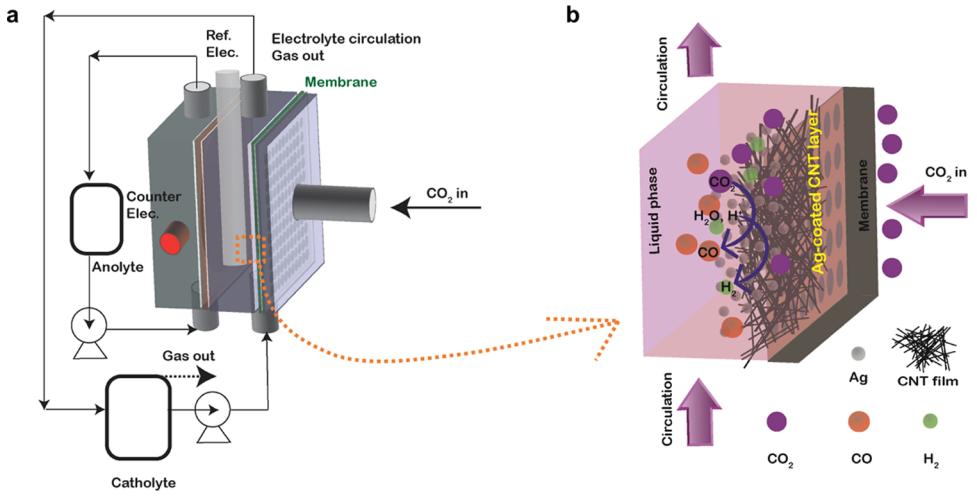

Figure 1. Overview of direct CO_2 delivery and conversion using electrocatalytic membranes. (a) Configuration of a CO_2 electrolyzer is used in this study. CO_2 is continuously purged into the electrolyzer, passing from the backside of the membrane to the electrolyte and the electroactive membrane interface. (b) Illustration of direct CO_2 delivery and conversion through the membrane. The Ag-coated CNT layer is utilized as active sites at the membrane−electrolyte interface for syngas production. CO_2 is converted into CO, accompanied by a H_2 evolution reaction.

economic value. Meanwhile, electrochemical generation of longer-chain products has been limited to very small quantities and the corresponding FEs are low.[13,14] Another challenge is that most research has been centered on material innovation and reactor optimization, using ideal aqueous electrolytes (e.g., $KHCO_3$, KOH) and organic solvents,[15,16] while a limited focus has been placed on practical considerations such as long-term material performance or the role of various ion species in nonideal CO_2R electrolytes that can fit into biological chain elongation.

In this context, the hybrid approach of integrating electrolysis with bioconversion presents a new pathway for generating long chain and more valuable carbon products with higher efficiencies. For instance, biocatalysis utilizes electroactive bacteria for CO_2 fixation, which generates C1−C6 carbons in a set of metabolic pathways (e.g., reductive acetyl-CoA, reductive tricarboxylic acid cycle).[17,18] It could achieve a higher FE of 21.8% for isopropanol generation in the hybrid system, far exceeding the highest reported 5.1% FE for the electrochemical production of 1-propanol.[13,14,19] However, there is still an inherent mismatch in electron supply rates from electrochemical reactions and microbial uptake rates for CO_2 upgrading. The microbial CO_2 conversion rates in microbial electrosynthesis (MES) are reported with values of 0.3−186 mg $CO_2/(cm^2$ day) (equivalent to 0.01−4.3 mM $e^-/(cm^2$ day)),[20] which are orders of magnitude slower than the electrochemical syngas production rates (5−500 mA/cm^2 for CO generation at ≥90% FE, equivalent to 2−220 mM $e^-/(cm^2$ day)).

This study presents a new integrated system that uses a novel catalytic membrane electrode to enable simultaneous electrotuning of syngas ratio (CO/H_2) and in situ direct delivery in the aqueous biocompatible electrolyte. The produced syngas can then be utilized as a gaseous feedstock for microbial upgrading,[21] which allows faster electron transfer than rate-limited direct extracellular transfer as well as producing more diverse products.[22] We aim to enable efficient hybrid CO_2 upgrading with CO generation toward artificial photosynthesis rather than outperforming state-of-the-art electrochemical syngas productions. Certain microbial communities can uptake H_2 as the electron donor to reduce CO_2 and thus produce organic chemicals.[23] CO itself can also be utilized as the electron donor and carbon source for upgrading (Supporting Information, theoretical equations). There are several advantages of microbial CO utilization over H_2 utilization. First, CO has a higher mass-transfer coefficient than H_2 in the media, which would allow easier utilization.[24] Second, as the electron donor, CO is more thermodynamically favorable than H_2 for contributing electrons to microbes.[25] Third, a higher CO concentration in the syngas may lead to more reduced products, such as ethanol over acetate.[26] Different from the traditional CO_2 gas feeding, which flows along the backside of the gas diffusion electrode (GDE) to achieve high current densities,[27] CO_2 gas was directly fed through the membrane to minimize syngas losses and match for slower microbial uptake rates. In addition to the ideal $KHCO_3$ electrolyte used in most CO_2RR systems, we also evaluated the impacts of more realistic electrolytes containing cell growth nutrients (e.g., NH_4Cl, yeast extract, and other ingredients) on syngas production. The results showed that such nutrient species could be influential in H_2 production and led to syngas composition change. The increasing nutrient concentration promotes H_2 evolution by offering significant amounts of proton sources.

EXPERIMENTAL SECTION

Preparation of Electrolytes. Initial electrolysis experiments were carried out using ideal 0.1 M $KHCO_3$ (99.7%, Sigma-Aldrich) electrolyte. To assess the electrocatalytic performance under a biocompatible electrolyte, PETC bacterial media was used as the electrolyte in anode and cathode chambers.[28] General salts and ingredients used for preparing PETC mineral media were 0.1 g of KCl (99−100.5%, Sigma-Aldrich), 0.2 g of $MgSO_4·7H_2O$ (100%, Fisher Chemical), 0.8 g of NaCl (99.8%, Fisher Chemical), 0.1 g of KH_2PO_4 (≥98%, Sigma-Aldrich), 0.02 g of $CaCl_2·2H_2O$ (≥99%, Fisher Chemical), 2 g of $NaHCO_3$ (99.5%, ACROS Organics), and 980 mL of DI water. NH_4Cl (≥99.0%, Fisher Chemical) and yeast extract (Molecular Genetics) were tested at various concentrations within a relevant range for bacterial growth.

Preparation of Electrocatalytic Membranes. Electrocatalytic membranes were fabricated in three steps: First, a hydrophobic poly(tetrafluoroethylene) membrane (PTFE, 90 mm in diameter, laminated, 0.1 μm, Sterlitech) was placed on the filter holder and wet

https://doi.org/10.1021/acssuschemeng.1c01150
ACS Sustainable Chem. Eng. 2021, 9, 6012−6022

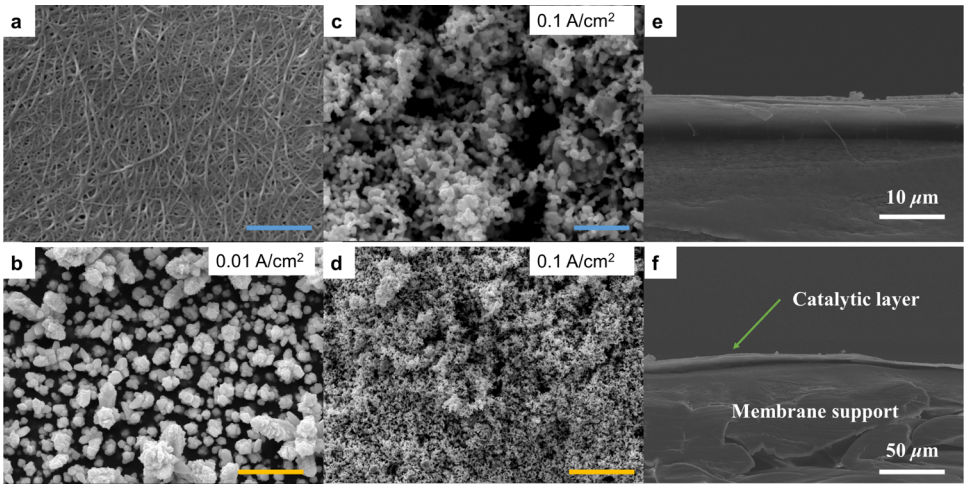

Figure 2. Microscopic view of electrocatalytic membranes. (a) Electroconductive CNT membrane with uniformly distributed CNT. (b) Ag−CNT membrane fabricated under the low current density (0.01 A/cm^2). (c, d) Ag−CNT membrane prepared under the high current density (0.1 A/cm^2) at different scales. Blue and yellow scale bars represent 1 and 5 μm, respectively. (e, f) Cross-sectional view of the fabricated electrocatalytic membrane.

by ethanol (99.5%, ACROS Organics) prior to vacuum filtration. Second, to obtain a uniform and porous CNT network, carbon nanotube (CNT) suspension was prepared by sonicating single−double-walled CNTs (Outer diameter: 1−4 nm, length 3−30 μm, >99%, Cheap Tubes Inc.) with surfactant sodium dodecyl sulfate (SDS, ≥99%, Fisher Chemical, for dispersing CNT effectively) in water, followed by centrifugation to minimize impurities and less conductive aggregates (30 min sonication, 0.1 g/L CNT, 10 g/L SDS, centrifuged at 13 000 g for 15 min twice; Branson Sonifier SFX250), and then 50 mL of suspension was filtrated to form a conductive layer on the membrane's surface. The as-prepared conductive membrane was then cleaned by filtrating deionized water (1 L) to remove the excess amount of SDS surfactant. CNT network is mainly used to provide high electrical conductivity for the current flow. At last, the membrane and a porous titanium mesh were used as the cathode and anode and placed in the electrolyte comprising of 2 M NH_4Cl, 1.5 M KSCN (≥99%, Arcos Organics), and 0.01 M $AgNO_3$ (0.0141 N, Ricca Chemical). Ag, as the core catalyst that drives the electrochemical syngas generation through CO_2 reduction and water/proton reduction, was electrodeposited on the membrane's surface at a specified current density under different reaction times.

Physical Characterization. The microscopic view of fabricated electrocatalytic membranes was obtained using scanning electron microscopy (SEM, XL30 FEG, Philips/FEI). The images were taken under 15 kV accelerating energy and 10 mm working distance. The average membrane pore size was obtained from top-view SEM images using ImageJ.[29] Surface elemental information was obtained using a K-α X-ray photoelectron spectrometer (XPS, Thermo Fisher) with Al Ka source. The scan size was controlled at 400 μm. The membrane's hydrophobicity was characterized by a contact angle goniometer (Model 250, ramé-hart) before and after modification.

Electrochemical Measurements and Gas Analysis in the Flow Cell. A potentiostat (PC4/3000, Gamry Instruments) was used to perform electrochemical characterizations (cyclic voltammetry, CV, chronoamperometry). Electrocatalytic membranes were placed in the custom-made flow cell (Figure 1a) as the cathode; Ag/AgCl (3 M KCl, CHI instrument) and Pt wire (0.25 mm in diameter, 50 cm in length) were used as the reference electrode and the anode, respectively. Cathode and anode chambers were separated using the anion-exchange membrane (AMI-7001, Membrane International). Electrical potentials were converted to the reversible hydrogen electrode using eq 1

$$E\ (\text{vs RHE}) = E\ (\text{vs Ag/AgCl}) + 0.210\,\text{V} + 0.0592\,\text{V} \times \text{pH} \quad (1)$$

Humidified CO_2 gas was purged through the backside of the membrane, transport across the membrane, and into the catholyte. The resulting gases were then collected using gas bags (Calibrated Instruments, Inc.) connected to the headspace of the catholyte bottle. Catholyte and anolyte were circulated at a flow rate of 80 mL/min using a peristaltic pump (Masterflex, Model: 7528-10). H_2 and CO were analyzed by manually injecting collected gases into gas chromatography (GC). Specifically, SRI 8610C was used for H_2 detection (SRI Instrument, injection volume: 0.1 mL, carrier gas: N_2),[11] and an Agilent 8890 GC system was used for CO analysis (Agilent Technology, injection volume: 0.05 mL, carrier gas: He). Faradic efficiency for each gas was calculated based on their partial current density with respect to the overall current density. All experimental results were done in triplicate, and error bars reflect the standard deviation among three measurements.

Quantification of Enhanced Hydrogen Evolution Reaction in Bioelectrolytes. The additional component NH_4Cl and yeast extract used in bioelectrolytes may serve as additional proton donors for H_2 evolution reaction. Equation 2 was expressed to represent the partial current density for the H_2 eovlution,[30] j_{HER}, where, k_1,k_2, and k_3 are reaction rate constants. β, β', and β'' are symmetry factors. E, F, R, and T are applied potential, faradaic constant, gas constant, and temperature, respectively. [HM] represents [NH_4^+] or potential proton donor sources from the yeast extract.

$$j_{HER} = k_1[HM]_e^{(-E)\beta F/RT} + k_2[H_2O]_e^{(-E)\beta' F/RT} + k_3[H^+]_e^{(-E)\beta'' F/RT} \quad (2)$$

RESULTS AND DISCUSSION

Electrocatalytic Membrane Fabrication. A thin film of CNT was first deposited on PTFE membranes through vacuum filtration to create a conductive substrate for subsequent Ag electrodeposition. The uniformity, porosity, and conductivity of the CNT layer are essential properties for consequent Ag electrodeposition and for facilitating gas conversion during CO_2 electrolysis. Prior to vacuum filtrating the CNT suspension, it was crucial to prewet the PTFE membrane to avoid hydrophobic portions that may result in a nonuniform CNT coating layer. As shown in Figure 2a, the as-formed CNT layer was relatively uniform and dense, showing a porous structure with an average pore size of 32 ± 6 nm (in diameter, characterized by ImageJ).[29] A cross-sectional view

https://doi.org/10.1021/acssuschemeng.1c01150
ACS Sustainable Chem. Eng. 2021, 9, 6012−6022

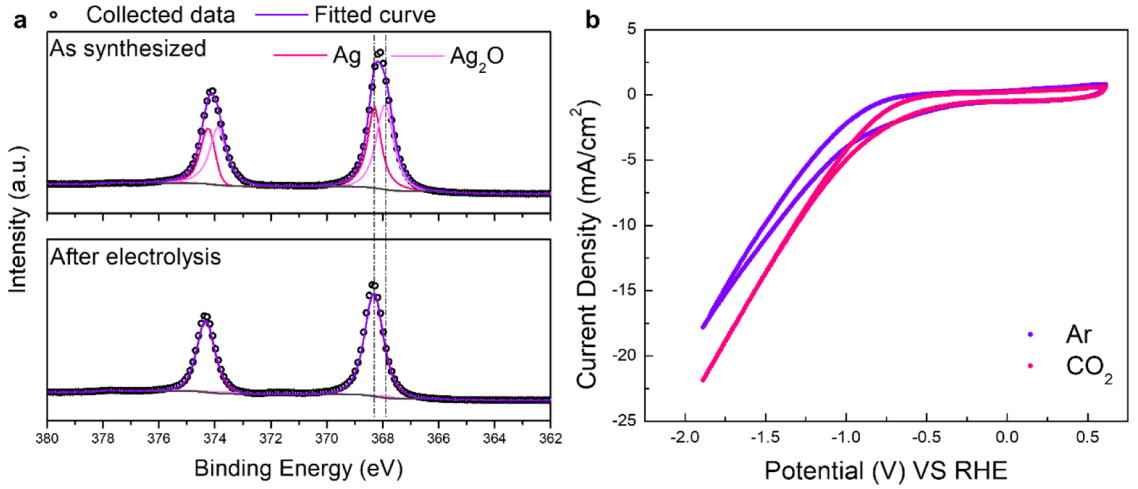

Figure 3. Structural and performance characterization. (a) XPS analysis shows the chemical state of the Ag peak. A dramatic decrease of the Ag_2O peak (light magenta) was observed before and after electrolysis, which was converted to the Ag peak (pink). (b) Cyclic voltammetry analysis of the prepared membrane in 0.1 M $KHCO_3$ electrolyte. The electrolyte was purged with Ar (violet) and CO_2 (pink) before electrolysis and was still under continuous purging during electrolysis.

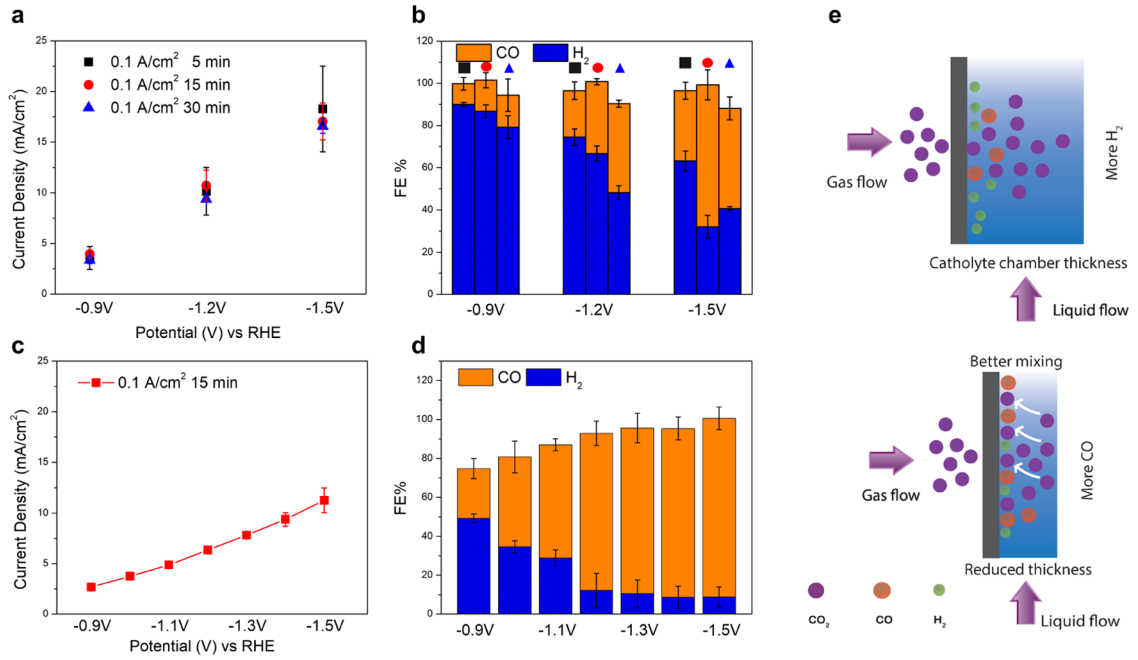

Figure 4. Electrochemical CO_2 reduction to tunable syngas mixes in two CO_2 electrolyzers with different catholyte chamber thickness. (a, b) Current density, faradic efficiency, and CO/H_2 ratios of different electrocatalytic membranes using the CO_2 electrolyzer with 2 cm catholyte chamber thickness. Black square, red circle, and blue triangle correspond to membranes fabricated under different electrodeposition times of 5, 15, and 30 min, respectively. (c, d) Current density and faradic efficiency, and CO/H_2 ratios of the electrocatalytic membrane (15 min) using the CO_2 electrolyzer with 1 cm catholyte chamber thickness. (e) Illustration of reduced catholyte chamber thickness resulted in CO_2 gas bubbles redistributed back to the electrode surface under better mixing and thus promoted the CO_2 reduction to CO while lowered H_2 evolution in this direct gas delivery system. The gas delivery rate was controlled at 2.5 sccm, and 0.1 M $KHCO_3$ was used as the electrolyte.

(Figure 2e,f) of the CNT layer showed a thickness of 3−5 μm, which contributed to a low resistance of 12.9 ± 2.9 Ω at a 3 cm distance.

Previous studies reported that Ag foam can be deposited on metal surfaces under high current densities,[31,32] so in this study, we used a similar approach for Ag deposition on the porous CNT layer. When the electrolyte containing highly concentrated NH_4Cl, the Ag reduction process involves a H_2 reaction, promoting the formation of a foamlike structure.[31] As such, current density plays an essential role in determining the morphology of the Ag layer as it directly controls the rate of H_2 formation. At a low current density of 0.01 A/cm^2, micron-sized Ag particles were formed on the surface (Figure 2b), indicating insignificant H_2 evolution. In contrast, a higher current density of 0.1 A/cm^2 created nanoporous Ag on the surface (Figure 2c,d), likely due to increased H_2 bubble formation during deposition. It has been noted that polycrystalline (micron-sized) Ag is much less effective for CO_2RR than nanoporous Ag, due to its less curved surface, lower activity, and smaller surface area.[33] Therefore, the

https://doi.org/10.1021/acssuschemeng.1c01150
ACS Sustainable Chem. Eng. 2021, 9, 6012−6022

nanoporous Ag layer formed under the higher current density was preferred for subsequent CO_2RR experiments. Further catalyst morphology optimization was made via deposition time variation. The formation of the Ag layer was characterized under deposition times of 5, 15, and 30 min, respectively, and SEM images showed that all surfaces were covered with the porous Ag layer, but the surface coverage and the size of Ag particles varied with time (Figure S1). In general, the 15 min deposition time could provide slightly better surface coverage than 5 min, but a longer deposition time of 30 min led to the formation of submicron-sized Ag particles. As confirmed by contact angle measurement, the membrane's surface also turned to be more hydrophilic after electrodeposition (113 ± 8 to 49 ± 7°, Figure S2).

Nanoporous Ag Membrane CO_2RR Performance and Tunable Syngas Production. The existence of Ag catalysts on the electrocatalytic membrane surface was verified by XPS analysis before and after CO_2RR. Figure 3a shows two distinctive Ag peaks (black dots) in both the as-synthesized membrane and the membrane after electrolysis. The fitting result (violet line) demonstrated the coexistence of elemental Ag (pink line) and Ag_2O (light magenta line) on the as-synthesized membrane surface, whose binding energy was at 368.3 (Ag $3d_5$) and 367.9 eV (Ag_2O $3d_5$), respectively. After 10 h electrolysis, the two peaks were shifted slightly and the Ag_2O peak in the fitted data was diminished, which was attributed to the electrochemical reduction of Ag_2O to Ag on the surface during electrolysis,[32] benefiting subsequent CO_2RR.

CV was first conducted to examine the membrane's efficacy for the CO_2RR. An aqueous electrolyte of 0.1 M $KHCO_3$ was presaturated with Ar and CO_2 under continuous purging. The CV curve for the CO_2 saturated electrolyte (Figure 3b, pink line) showed a sharp enhancement of current density at potentials lower than −0.7 V (vs RHE) when comparing to the Ar-saturated electrolyte (Figure 3b, violet line), indicating that the additional surface adsorbed CO_2 (aq) was electrochemically converted to reduced products. Overall, the enhancement of current density confirms that the CO_2RR process started at −0.7 V (vs RHE), with lower potentials contributing more CO_2RR.

The performance of the as-prepared membranes for tunable syngas (CO/H_2) production was examined in 0.1 M $KHCO_3$ using a custom-built CO_2 electrolyzer with a 2 cm thick catholyte chamber. All membranes exhibited increased current density with decreasing potential, with reported values of 3, 10, 17 mA/cm^2 at potentials ranging from −0.9, −1.2, and −1.5 V, respectively (Figure 4a). Additionally, regardless of the electrodeposition times used to prepare the Ag foams, similar current densities were observed. In contrast, the longer Ag deposition time led to higher CO production when comparing 5 min case (black squares) to 15 and 30 min cases (red circles and blue triangles) under each applied potential. This is possibly due to the higher Ag loading and coverage on the membrane surface allows for better CO_2RR. In addition, reducing the electrical potential showed a direct correlation with increased CO/H_2 ratio, which indicates that the syngas mix composition can be tuned using this process (Figure 4b). For example, the CO/H_2 ratio for the 15 min case increased from 12:88 to 41:59 when the potential was reduced from −0.9 to −1.5 V, and the trend was consistent under different current densities and deposition times.

During the direct CO_2 delivery process, gases pass through the membrane unevenly due to the nonuniform pore size distributions. To increase local CO_2 availability for improved CO_2RR and obtain higher efficiency, lower channel thickness was tested by reducing the space from 2 to 1 cm with one deposition condition of 0.1 A/cm^2 for 15 min. Slightly lower current densities were observed, with reported values of 3, 6, and 11 mA/cm^2 at potentials of −0.9, −1.2, and −1.5 V (vs RHE), respectively (Figure 4c). However, much higher FEs for CO were obtained in the narrower chambers across the potential range tested. For example, higher values of 25% (vs 22%) and 92% (vs 42%) were shown at both the higher (−0.9 V vs RHE) and the lower (−1.5 V vs RHE) limit potentials compared to the 2 cm setup (Figure 4d).

More interestingly, the thinner chamber expanded the range tunability of the syngas mix between H_2 and CO. In the thicker CO_2 electrolyzer (~2 cm), as potentials decreased from −0.9 to −1.5 V for membranes fabricated under 15 min deposition time, production rates increased from 0.03 to 0.07 mL/(min cm^2) for H_2, and 0.004−0.05 mL/(min cm^2) for CO, respectively (Figure S3). Correspondingly, the produced gas ratios increased from 1 to 4% for H_2 and 0.2 to 3% per cm^2 for CO, which represented an increasing syngas ratio (CO/H_2) from 12:88 to 41:59 (Figure 4b). When using a thinner CO_2 electrolyzer (~1 cm), H_2 production rates (~0.01 mL/(min cm^2)) remained relatively consistent among the tested potential range (−0.9 to −1.5 V), while the CO production rate was consistently increasing from 0.005 to 0.08 mL/(min cm^2) with decreasing potentials from −0.9 to −1.5 V. As a result, the gas ratio in the gas permeate for H_2 was remained ~0.5% per cm^2, while CO had an increasing ratio from 0.3 to 5% per cm^2. This led to an increasing syngas ratio from 35:65 to almost 91:9, respectively (Figure 4d). Overall, the lower potentials promoted both higher syngas ratios and the thinner chamber electrolyzer produced more CO and its syngas mixtures were more CO-weighted (>50%), while the thicker chamber electrolyzer generated more H_2-weighted mixture with syngas ratio <50%, making the two designed complementary to each other yet both were responsive to electrochemical tuning. As summarized in Table S1, most Ag-based electrochemical CO_2 reduction to CO studies are operated in the standard H-cell configuration or flow cells with CO_2 gas flow-by on the backside of the electrode, making them difficult for direct comparison. For example, different types of Ag were tested in the H-cells using the pure $KHCO_3$ electrolyte, which achieved maximum faradic efficiencies of 78−92% and current densities of 4−18 mA/cm^2 under optimal potentials (−0.6−1.1 V vs RHE).[33−35] However, those processes are not ideal for long-term operations. Thus, flow cells with catalysts immobilized on the gas diffusion electrodes were also used to achieve high current densities (85−100 mA/cm^2), stable long-term performance (10−24 h), and high FEs (75−94%).[36−38] Some flow cell systems use alkaline solution (10 M KOH) or operate in the gas-phase CO_2 electrolysis setup,[36,37] making them impossible for microbial integration. Similar to this study, previous research also investigated the direct delivery of CO_2 through Ag net for direct electrochemical CO generation, which achieved a maximum FE of 90% at the potential of −1.6 V vs RHE, followed by a gradual decline of CO FE to 50% in 5 h.[39] In contrast, this system offers much longer long-term stability (144 h) at 92% FE and 1.5 V vs RHE potential, making it applicable for long-term MES studies.

https://doi.org/10.1021/acssuschemeng.1c01150
ACS Sustainable Chem. Eng. 2021, 9, 6012−6022

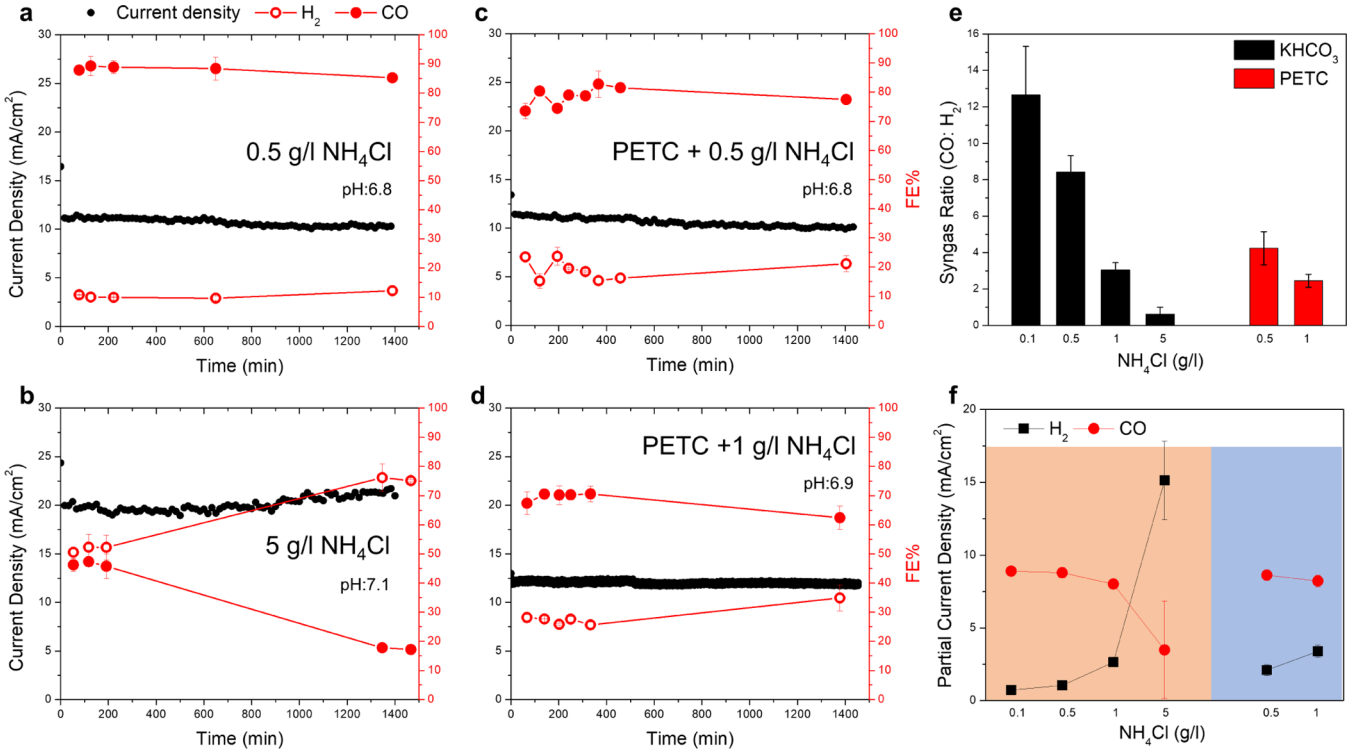

Figure 5. NH_4Cl concentration impacts on the long-term CO_2 electrolysis performance. (a–d) Electrolysis performance of the electrocatalytic membrane using 0.1 M (10 g/L) $KHCO_3$ and simulated microbial dilute media (PETC) under different NH_4Cl concentrations. Black dots, red open dots, and red solid dots represent current density, H_2, and CO faradic efficiencies. (e) Effect of NH_4Cl concentration on generated syngas ratio during long-term electrolysis. Black and red bars represent the bulk electrolytes are 0.1 M $KHCO_3$ and PETC. (f) Partial current densities of H_2 and CO during long-term electrolysis. Orange and blue zones represent the major electrolytes 0.1 M $KHCO_3$ and PETC minerals. Black dots and red dots represent H_2 and CO partial current densities.

The increase in CO FE in the thinner chamber (~1 cm) was believed to be attributed to the increased local CO_2 concentration along the membrane surface. During the CO_2 gas delivery process, CO_2 gas was fed on the backside of the membrane, which then preferentially passed through a particular region rather than the whole membrane due to the nonuniform pore size distribution, leading to the noneven distribution of adsorbed CO_2 gas on the electrode surface. Although the CO_2 feeding was on the backside of the membrane, and its transport across the membrane was not directly influenced by the chamber thickness, the smaller chamber thickness promoted stronger hydraulic shearing created by the liquid circulation (larger Reynolds number), which facilitated the more even distribution of CO_2 gases along the membrane active surface. Therefore, it is likely that the reduced thickness helped CO_2 that already transported across the membrane pores to redistribute more evenly on the active membrane (electrode) surface, thus overcoming the local CO_2 concentration deficiency and allowing for much higher CO FEs (Figure 4e). This mechanism is further supported by a previous study conducting electrochemical CO_2 reduction to formate. It demonstrated that reduced channel thickness increased the Reynolds number of the liquid electrolyte crossing the channel, which created more mixing and resulted in increased faradic efficiency.[40]

Different gas delivery rates of 1 and 5 standard cubic centimeters per minute (sccm) were tested to further optimize syngas production on the electrocatalytic membranes using the 1 cm thick chamber electrolyzer (Figure S4). The FE and gas production rates for CO and H_2 of both 1 and 5 sccm cases were similar when comparing to 2.5 sccm. At 1 sccm, FE for CO increased from 31 to 83%, while H_2 FE decreased from 67 to 14% when the potential decreased from −0.9 to −1.5 V. At the elevated 5 sccm, FE for CO increased from 29 to 82%, while FE for H_2 decreased from 56 to 11% at the same tested potential range. However, gas ratios in the permeate were higher at lower delivery rates due to a greater dilution from excess CO_2. At the fastest delivery rate of 5 sccm, the system operated at −0.9 to −1.5 V only generated H_2 and CO at 0.2–0.4 and 0.2–2.3% per cm^2, respectively, while at the lowest rate of 1 sccm, higher H_2 and CO contents of 1.1–1.5 and 0.7–8% per cm^2 were observed. Therefore, the gas delivery rates tested in the system did not have a significant impact on the electrochemical reactions, which only affected the gas ratio in the permeate due to the excess amount of CO_2.

The current density numbers using this flow-through mode were lower than studies using traditional flow-by gas delivery for CO_2RR. This is likely due to the direct purging of CO_2 through the membrane created surface bubbles that reduced the contact area and ion flow between the electrode surface and liquid electrolyte. This likely leads to increased overpotentials and the observed lower current densities.[41] In line with these findings, a ca. 80% drop in current density (18 vs 3 mA/cm^2 at −0.9 V) was observed when there was a small pressure built up on the backside of the membrane (~0.5 psi, Figure S5). However, achieving high current density was not the goal of this study, rather we hoped to develop an electrochemical CO_2RR system that can generate tunable syngas product with a current density suitable for the downstream biological upgrading process. With this in mind,

https://doi.org/10.1021/acssuschemeng.1c01150
ACS Sustainable Chem. Eng. 2021, 9, 6012–6022

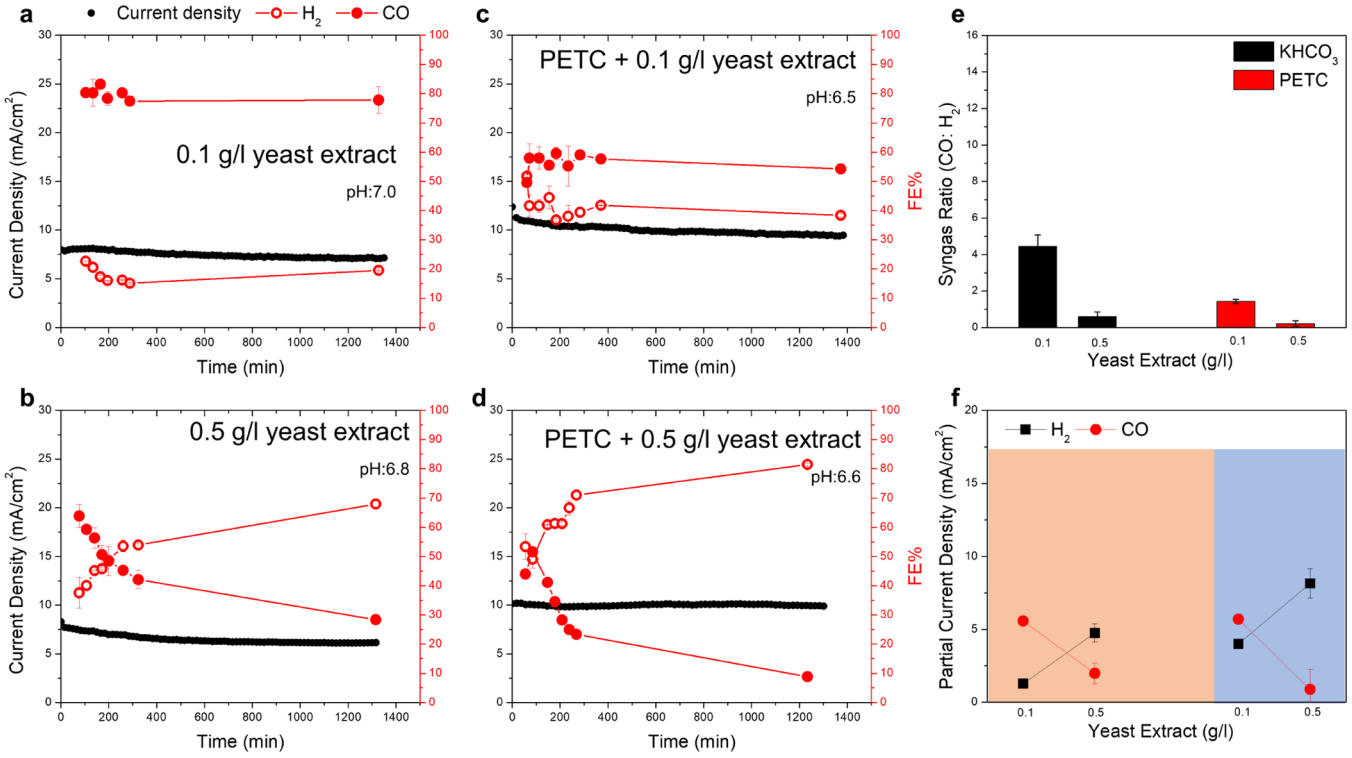

Figure 6. Yeast extract concentration impacts on the long-term electrolysis performance. (a, b) Electrolysis performance of the electrocatalytic membrane using 0.1 M (10 g/L) $KHCO_3$ and varied yeast extract concentrations. (c, d) Electrolysis performance in simulated microbial dilute media (PETC) with varied yeast extract concentrations. Black dots, red open dots, and red solid dots represent current density, H_2, and CO faradic efficiencies, respectively. (e) Effect of yeast extract concentration on the generated syngas ratio during long-term electrolysis. Black and red bars represent the bulk electrolytes are 0.1 M $KHCO_3$ and PETC. (f) Partial current densities of H_2 and CO during long-term electrolysis. Orange and blue zones represent the major electrolytes 0.1 M $KHCO_3$ and PETC minerals. Black dots and red dots represent H_2 and CO partial current densities.

considering the reported current densities in biocatalytic CO_2RR systems are much lower at ~1 mA/cm^2,[19,42,43] the current density observed in this direct flow-through mode already exceeds these limits and may be efficient for the downstream biological reactions.

Impacts of Key Microbial Growth Ingredients on CO_2 Reduction to Syngas. Most electrocatalytic CO_2 reduction studies used pure bicarbonate and hydroxide electrolytes, which are not compatible with the bioconversion process due to deficiency of necessary nutrients and extreme pHs.[44,45] To connect electrocatalysis with bioupgrading, some nutrients such as NH_4Cl and yeast extract are important for cell growth, but few studies tested how such ingredients affect the electroreduction.[46] Therefore, as a critical step of integration, we first tested CO_2RR conducted in ideal 0.1 M $KHCO_3$ electrolyte with increasing NH_4Cl concentrations (Figures 5a,b and S6). As expected, the current density increased with increasing NH_4Cl concentration due to higher ionic strengths, and the overall CO and H_2 FE was >90%, indicating high efficiency for syngas production. However, higher NH_4Cl concentrations promoted H_2 evolution. When the NH_4Cl concentration was under 0.5 g/L, FEs for CO and H_2 were relatively stable (Figures 5a and S6a). Accordingly, FE for CO remained ~85 to 90% and the FE for H_2 was steadily below 15%, representing syngas ratios CO/H_2 of 93:7 and 89:11, respectively (Figure 5e). When NH_4Cl concentration was increased to 1 g/L (Figure S6b), FE for H_2 was increased to 20−30%, while the FE for CO dropped to 70−80%, resulting in a decrease in syngas ratio of CO/H_2 of 75:25 (Figure 5e). When NH_4Cl concentration was further increased to 5 g/L (Figure 5b), FE for H_2 surpassed the case for CO, starting at ~50 to 55% and gradually increasing to ~75%. In contrast, FE for CO decreased slowly from ~50 to ~20% within 24 h, resulting in a lower syngas ratio of CO/H_2 (39:61) (Figure 5e). The current of H_2 evolution can be considered as the summation of current contributed by three major proton donors of NH_4^+, H^+, and H_2O (eq 2).[30]

Furthering this characterization, a widely used and more complex microbial growth medium PETC was tested for CO_2RR. PETC is commonly used for culturing acetogens that are capable of utilizing syngas (H_2/CO/CO_2) for growth via the Wood−Ljungdhal pathway and produce carboxylic acids.[26,47] The minimum PETC media contains salts such as KCl, $MgSO_4$, NaCl, KH_2PO_4, $CaCl_2$, and $NaHCO_3$ and nutrient elements such as NH_4Cl (~1 g/L) and yeast extract (~1 g/L). Figure 5c,d shows the CO_2 electrolysis in PETC media (excluding yeast extract) at different NH_4Cl concentrations. It shows electrolysis was less effective for CO production in PETC than ideal 0.1 M $KHCO_3$, while a similar trend of reduced CO but increased H_2 was observed in increasing NH_4Cl concentration in PETC. From 0.5 to 1 g/L NH_4Cl, FE for H_2 increased by ~15%, while FE for CO dropped by ~15%, which caused the decreased CO/H_2 ratio from 81:19 to 71:29 (Figure 5e).

The dynamic change of FE on CO and H_2 in PETC is believed attributed to the availability of proton donors (e.g., NH_4^+, H^+, H_2O). Typically, H^+ itself and H_2O served as proton donors for H_2 evolution in the ideal bicarbonate-based

https://doi.org/10.1021/acssuschemeng.1c01150
ACS Sustainable Chem. Eng. 2021, 9, 6012−6022

aqueous CO_2RR process, and water, in particular, was the primary proton donor as H^+ reduction was diffusion-limited and highly dependent on the concentration, even at the low pH of 2.5.[48] Adding NH_4^+ into the CO_2RR process generated more H_2 because NH_4^+ itself was also a proton donor. It undergoes dissociation at high pHs and is easier than water to be utilized as the proton donor source (eq 3).

$$[NH_4^+] = [NH_3] + [H^+]\ pK_a = 9.2 \quad (3)$$

As the concentrations of NH_4^+ increased from 2 to 93 mM (equivalent to 0.1−5 g/L NH_4Cl), it provided far higher availability of protons for H_2 evolution than the readily available H^+ from the electrolyte pH ($(\sim 8 \text{ to } 16) \times 10^{-5}$ mM). In addition, the electrochemical reduction happening on the electrode surface may drive pH exceeding the pK_a value of 9.2, which promoted the release of $[H^+]$ for subsequent H_2 evolution. Similar to H^+, NH_4^+ was less efficient for enhancing H_2 evolution at the low concentration range (2−9 mM) because of local concentration deficiency. However, higher NH_4^+ concentrations (19−93 mM) reduced mass-transfer limitation and better served as the proton donor, facilitating H_2 evolution (higher FE for H_2). Therefore, we can conclude from the expression that the partial current density for H_2 evolution is highly dependent on the NH_4^+ concentration (Figure 5f), while the latter two terms in eq 2 are quite constant because of the same water concentration and the relatively stable pH in Figures 5a,b and S6. Additionally, the electrode surface is inevitably poisoned by trace metal ions from the PETC electrolyte during long-term operations. XPS analysis demonstrated that both Zn and Cu were appeared on the surface after electrolysis (Figure S7). Those poisoning effects could also lead to more H_2 evolution during electrolysis.

Yeast extract is a key ingredient in the PETC and many cell growth media, but its impacts on CO_2 electrolysis also remain unknown.[49,50] Yeast extract is a complex mixture of many micronutrient species, including acidic species such as nucleic acids and amino acids with low pK_a values, which could benefit H_2 evolution. We assessed the yeast extract impact on the electrolysis process both in the ideal 0.1 M $KHCO_3$ and PETC electrolytes. Overall, yeast extract behaved similarly to NH_4Cl, as increasing its concentration led to higher H_2 evolution than CO production. In general, its current densities were lower than the case of NH_4Cl, which may be caused by electrode surface fouling. In $KHCO_3$ electrolyte, CO and H_2 were consistently produced at ∼80 and ∼20% FE, respectively, under 0.1 g/L yeast extract concentration, yielding a CO/H_2 ratio of 82:18 (Figure 6e) with no significant fluctuations (Figure 6a). At the elevated concentration of 0.5 g/L, H_2 evolved quickly from accounting for ∼30 to ∼70% FE in ∼24 h operation. In the meantime, the FE for CO was also dropped from ∼70 to ∼30% accordingly (Figure 6b). This led to the CO/H_2 ratio dropped from 82:18 to 37:63 (Figure 6e). As a comparison to the $KHCO_3$ electrolyte, adding yeast extract into the PETC electrolyte led to an essentially identical trend. A low-range concentration of 0.1 g/L resulted in stable FEs of CO and H_2 at ∼55 and ∼40%, respectively (Figure 6c). The high concentration of 0.5 g/L, likewise, brought on a dynamic change of FE for H_2 from ∼50 to 80%, and FE for CO from ∼50 to 10% (Figure 6d). This overall led to a decreased CO/H_2 ratio from 59:41 to 18:82 (Figure 6e). Similar to NH_4Cl, yeast extract contains a variety of amino acids that can serve as efficient proton donors with low pK_a values, thus promoting H_2 evolution. Moreover, due to its complex composition, the electrode surface poisoning was more severe than the NH_4Cl case and resulted in Zn deposition (Figure S7). As confirmed by partial current densities (Figure 6f), the electrolysis was shifted more significantly to promote H_2 evolution over CO production with increasing yeast concentrations.

To further examine other possible mechanisms that resulted in such a dramatic drop, XPS analysis was conducted to examine possible surface contaminations. Different elemental peaks including N, Cu, and Zn were comparatively scanned among different samples and shown in Figure S7. Prolonged electrolysis demonstrated a dramatic increase of the N peak (Figure S7a), particularly in the yeast extract electrolyte, while the NH_4Cl case had a smaller and insignificant peak. This suggested that more N-rich components (e.g., amino acids, proteins) in yeast extract were irreversibly adsorbed on the membrane surface, in a larger amount than NH_4^+. This is because the adsorbed NH_4^+ from NH_4Cl may dissociate into NH_3 and H^+ under high local pHs, where NH_3 can be easily discharged from the membrane surface.[51] Both trace metal elements Cu and Zn were detected in the electrolyte. Figure S7b shows the Cu peak and suggested Cu existence in both electrolytes, which originated from the impurities of the chemical or yeast extract itself used. Moreover, Figure S7c shows Zn accumulation in the yeast extract electrolyte, indicating a relatively considerable amount of Zn was contained in the yeast extract, where the NH_4Cl case has a negligible amount of Zn deposition. Previous studies have shown that, even in the highest purity $KHCO_3$ (99.9999%) electrolyte, the existing trace metal ion impurities (Zn^{2+} and Cu^{2+}) were deposited on the Ag surface during electrolysis, leading to the loss of CO_2RR selectivity, benefiting H_2 evolution on the poisoned surfaces.[52] It may suggest that the surface poisoning effect would happen at higher concentrations as the CO production gradually dropped for the prolonged electrolysis (Figures 5b,d and 6b,d). However, the trace metal poisoning that resulted in the higher H_2 reaction seems less likely because the membrane's high selectivity toward CO could be recovered back when the electrolyte was switched back to the pure $KHCO_3$ electrolyte (Figure S8).

CONCLUSIONS

The integrated electrocatalytic membrane electrode could provide flexible syngas feedstock from CO_2 with tunable CO/H_2 ratios, which greatly expands the adaptability to downstream syngas bioconversion to value-added chemicals. The nontraditional flow-through feeding reduced loss matched for slower microbial uptake rates, and it could deliver syngas mix with CO/H_2 ratio ranging from 35:65 to 91:9 in the common $KHCO_3$ electrolyte. The biocompatible electrolytes containing multiple proton donors such as NH_4Cl and yeast extract favored more H_2 evolution, revealing the need of developing electrocatalytic processes that are resilient to actual electrolytes used in bioconversions. However, Ag is commonly used as an antimicrobial agent for disinfection primarily due to the Ag^+ release and the generation of reactive oxygen species under aerobic conditions. The study has shown that Ag NP exhibits minimal antibacterial activity under the anaerobic condition, which minimized Ag oxidation and the subsequent Ag^+ release under acidic conditions.[53] In our electrochemical system, the cathode chamber is controlled under an anaerobic condition with continuous CO_2 purging because the target syngas oxidizing bacteria (*Clostridium* strains) are anaerobic. Additionally, the cathodic reduction condition would also minimize

https://doi.org/10.1021/acssuschemeng.1c01150
ACS Sustainable Chem. Eng. 2021, 9, 6012−6022

the Ag^+ release from the electrode surface. Thus, our system can provide benign media for microbial growth with negligible antibacterial activity. This study brings possibilities for integrating electrochemical and biological processes to enable CO_2 upgrading and chain elongation. Further studies should include microbial conversion linking the electrocatalysis for in situ CO_2 reductions and syngas to chemical conversion.

■ ASSOCIATED CONTENT

Supporting Information

The Supporting Information is available free of charge at https://pubs.acs.org/doi/10.1021/acssuschemeng.1c01150.

Microscopic view of the electrocatalytic membrane fabricated under different reaction times; hydrophobicity of the membrane before and after modification; comparative table of Ag-based CO_2 electrolyzers for CO generation; electrocatalytic production of syngas using different electrolyzers; electrocatalytic performance of syngas production under different gas delivery rates; effect of operational mode on current density during chronoampermetry study; additional NH_4Cl concentration impacts on the long-term CO_2 electrolysis performance; XPS analysis of surface elemental contamination; continuous long-term testing with periodic $KHCO_3$ cleaning; and theoretical equations of syngas conversion to organic chemicals (PDF)

■ AUTHOR INFORMATION

Corresponding Author

Zhiyong Jason Ren − *Department of Civil and Environmental Engineering and the Andlinger Center for Energy and the Environment, Princeton University, Princeton, New Jersey 08544, United States;* orcid.org/0000-0001-7606-0331; Phone: +1(609)258 7580; Email: zjren@princeton.edu

Authors

Xiaobo Zhu − *Department of Civil and Environmental Engineering and the Andlinger Center for Energy and the Environment, Princeton University, Princeton, New Jersey 08544, United States*

Joshua Jack − *Department of Civil and Environmental Engineering and the Andlinger Center for Energy and the Environment, Princeton University, Princeton, New Jersey 08544, United States*

Yanhong Bian − *Department of Civil and Environmental Engineering and the Andlinger Center for Energy and the Environment, Princeton University, Princeton, New Jersey 08544, United States*

Xi Chen − *Department of Civil and Environmental Engineering and the Andlinger Center for Energy and the Environment, Princeton University, Princeton, New Jersey 08544, United States;* orcid.org/0000-0003-2360-2672

Nicolas Tsesmetzis − *New Energies Research and Technology, Shell International Exploration and Production Inc., Houston, Texas 77082, United States;* orcid.org/0000-0001-5246-0568

Complete contact information is available at: https://pubs.acs.org/10.1021/acssuschemeng.1c01150

Notes

The authors declare no competing financial interest.

■ ACKNOWLEDGMENTS

We appreciate the supports from Shell-National Renewable Energy Laboratory (NREL) under Subcontract No. 000034161 and a seed innovation grant from the Andlinger Center for Energy and the Environment at Princeton University. We thank Dr. Jonathan Lo and Dr. Wei Xiong for the valuable discussions. We also acknowledge the use of Princeton's Imaging and Analysis Center, which is partially supported through the Princeton Center for Complex Materials (PCCM), a National Science Foundation (NSF)-MRSEC program (DMR-2011750).

■ REFERENCES

(1) Global Monitoring Laboratory - Carbon Cycle Greenhouse Gases. https://www.esrl.noaa.gov/gmd/ccgg/trends/ (accessed Dec 1, 2020).

(2) van Aalst, M. K. The Impacts of Climate Change on the Risk of Natural Disasters. *Disasters* **2006**, *30*, 5−18.

(3) Li, B.; Duan, Y.; Luebke, D.; Morreale, B. Advances in CO_2 Capture Technology: A Patent Review. *Appl. Energy* **2013**, *102*, 1439−1447.

(4) Artz, J.; Müller, T. E.; Thenert, K.; Kleinekorte, J.; Meys, R.; Sternberg, A.; Bardow, A.; Leitner, W. Sustainable Conversion of Carbon Dioxide: An Integrated Review of Catalysis and Life Cycle Assessment. *Chem. Rev.* **2018**, *118*, 434−504.

(5) Ross, M. B.; De Luna, P.; Li, Y.; Dinh, C. T.; Kim, D.; Yang, P.; Sargent, E. H. Designing Materials for Electrochemical Carbon Dioxide Recycling. *Nat. Catal.* **2019**, *2*, 648−658.

(6) Birdja, Y. Y.; Pérez-Gallent, E.; Figueiredo, M. C.; Göttle, A. J.; Calle-Vallejo, F.; Koper, M. T. M. Advances and Challenges in Understanding the Electrocatalytic Conversion of Carbon Dioxide to Fuels. *Nat. Energy* **2019**, *4*, 732−745.

(7) Hori, Y.; Wakebe, H.; Tsukamoto, T.; Koga, O. Electrocatalytic Process of CO Selectivity in Electrochemical Reduction of CO_2 at Metal Electrodes in Aqueous Media. *Electrochim. Acta* **1994**, *39*, 1833−1839.

(8) Wu, J.; Sharifi, T.; Gao, Y.; Zhang, T.; Ajayan, P. M. Emerging Carbon-Based Heterogeneous Catalysts for Electrochemical Reduction of Carbon Dioxide into Value-Added Chemicals. *Adv. Mater.* **2019**, *31*, No. 1804257.

(9) Lu, L.; Guest, J. S.; Peters, C. A.; Zhu, X.; Rau, G. H.; Ren, Z. J. Wastewater treatment for carbon capture and utilization. *Nat. Sustainability* **2018**, *1*, 750−758.

(10) Windle, C. D.; Perutz, R. N. Advances in Molecular Photocatalytic and Electrocatalytic CO_2 Reduction. *Coord. Chem. Rev.* **2012**, *256*, 2562−2570.

(11) Lu, L.; Li, Z.; Chen, X.; Wang, H.; Dai, S.; Pan, X.; Ren, Z. J.; Gu, J. Spontaneous Solar Syngas Production from CO_2 Driven by Energetically Favorable Wastewater Microbial Anodes. *Joule* **2020**, *4*, 2149−2161.

(12) Kibria Nabil, S.; McCoy, S.; Kibria, M. G. Comparative Life Cycle Assessment of Electrochemical Upgrading of CO_2 to Fuels and Feedstocks. *Green Chem.* **2021**, *23*, 867−880.

(13) Grim, R. G.; Huang, Z.; Guarnieri, M. T.; Ferrell, J. R.; Tao, L.; Schaidle, J. A. Transforming the Carbon Economy: Challenges and Opportunities in the Convergence of Low-Cost Electricity and Reductive CO_2 Utilization. *Energy Environ. Sci.* **2020**, *13*, 472−494.

(14) Zhuang, T. T.; Liang, Z. Q.; Seifitokaldani, A.; Li, Y.; De Luna, P.; Burdyny, T.; Che, F.; Meng, F.; Min, Y.; Quintero-Bermudez, R.; Dinh, C. T.; Pang, Y.; Zhong, M.; Zhang, B.; Li, J.; Chen, P. N.; Zheng, X. L.; Liang, H.; Ge, W. N.; Ye, B. J.; Sinton, D.; Yu, S. H.; Sargent, E. H. Steering Post-C-C Coupling Selectivity Enables High Efficiency Electroreduction of Carbon Dioxide to Multi-Carbon Alcohols. *Nat. Catal.* **2018**, *1*, 421−428.

(15) Kibria, M. G.; Edwards, J. P.; Gabardo, C. M.; Dinh, C. T.; Seifitokaldani, A.; Sinton, D.; Sargent, E. H. Electrochemical CO_2 Reduction into Chemical Feedstocks: From Mechanistic Electro-

catalysis Models to System Design. *Adv. Mater.* **2019**, *31*, No. 1807166.
(16) König, M.; Vaes, J.; Klemm, E.; Pant, D. Solvents and Supporting Electrolytes in the Electrocatalytic Reduction of CO_2. *iScience* **2019**, *19*, 135−160.
(17) Jiang, Y.; May, H. D.; Lu, L.; Liang, P.; Huang, X.; Ren, Z. J. Carbon Dioxide and Organic Waste Valorization by Microbial Electrosynthesis and Electro-Fermentation. *Water Res.* **2019**, *149*, 42−55.
(18) Salehizadeh, H.; Yan, N.; Farnood, R. Recent Advances in Microbial CO_2 Fixation and Conversion to Value-Added Products. *Chem. Eng. J.* **2020**, *390*, No. 124584.
(19) Arends, J. B. A.; Patil, S. A.; Roume, H.; Rabaey, K. Continuous Long-Term Electricity-Driven Bioproduction of Carboxylates and Isopropanol from CO_2 with a Mixed Microbial Community. *J. CO2 Util.* **2017**, *20*, 141−149.
(20) Bian, B.; Bajracharya, S.; Xu, J.; Pant, D.; Saikaly, P. E. Microbial Electrosynthesis from CO_2: Challenges, Opportunities and Perspectives in the Context of Circular Bioeconomy. *Bioresour. Technol.* **2020**, *302*, No. 122863.
(21) Asimakopoulos, K.; Gavala, H. N.; Skiadas, I. V. Reactor Systems for Syngas Fermentation Processes: A Review. *Chem. Eng. J.* **2018**, *348*, 732−744.
(22) Claassens, N. J.; Cotton, C. A. R.; Kopljar, D.; Bar-Even, A. Making Quantitative Sense of Electromicrobial Production. *Nat. Catal.* **2019**, *2*, 437−447.
(23) Bakonyi, P.; Peter, J.; Koter, S.; Mateos, R.; Kumar, G.; Koók, L.; Rózsenberszki, T.; Pientka, Z.; Kujawski, W.; Kim, S. H.; Nemestóthy, N.; Bélafi-Bakó, K.; Pant, D. Possibilities for the Biologically-Assisted Utilization of CO_2-Rich Gaseous Waste Streams Generated during Membrane Technological Separation of Biohydrogen. *J. CO2 Util.* **2020**, *36*, 231−243.
(24) Munasinghe, P. C.; Khanal, S. K. Evaluation of Hydrogen and Carbon Monoxide Mass Transfer and a Correlation between the Myoglobin-Protein Bioassay and Gas Chromatography Method for Carbon Monoxide Determination. *RSC Adv.* **2014**, *4*, 37575−37581.
(25) Hu, P.; Bowen, S. H.; Lewis, R. S. A Thermodynamic Analysis of Electron Production during Syngas Fermentation. *Bioresour. Technol.* **2011**, *102*, 8071−8076.
(26) Jack, J.; Lo, J.; Maness, P. C.; Ren, Z. J. Directing Clostridium Ljungdahlii Fermentation Products via Hydrogen to Carbon Monoxide Ratio in Syngas. *Biomass Bioenergy* **2019**, *124*, 95−101.
(27) Liang, S.; Altaf, N.; Huang, L.; Gao, Y.; Wang, Q. Electrolytic Cell Design for Electrochemical CO_2 Reduction. *J. CO2 Util.* **2020**, *35*, 90−105.
(28) Cotter, J. L.; Chinn, M. S.; Grunden, A. M. Ethanol and Acetate Production by Clostridium Ljungdahlii and Clostridium Autoethanogenum Using Resting Cells. *Bioprocess Biosyst. Eng.* **2009**, *32*, 369−380.
(29) Duan, W.; Ronen, A.; Walker, S.; Jassby, D. Polyaniline-Coated Carbon Nanotube Ultrafiltration Membranes: Enhanced Anodic Stability for in Situ Cleaning and Electro-Oxidation Processes. *ACS Appl. Mater. Interfaces* **2016**, *8*, 22574−22584.
(30) Jackson, M. N.; Jung, O.; Lamotte, H. C.; Surendranath, Y. Donor-Dependent Promotion of Interfacial Proton-Coupled Electron Transfer in Aqueous Electrocatalysis. *ACS Catal.* **2019**, *9*, 3737−3743.
(31) Cherevko, S.; Xing, X.; Chung, C. H. Electrodeposition of Three-Dimensional Porous Silver Foams. *Electrochem. Commun.* **2010**, *12*, 467−470.
(32) Dutta, A.; Morstein, C. E.; Rahaman, M.; Cedeno López, A.; Broekmann, P. Beyond Copper in CO_2 Electrolysis: Effective Hydrocarbon Production on Silver-Nanofoam Catalysts. *ACS Catal.* **2018**, *8*, 8357−8368.
(33) Lu, Q.; Rosen, J.; Zhou, Y.; Hutchings, G. S.; Kimmel, Y. C.; Chen, J. G.; Jiao, F. A Selective and Efficient Electrocatalyst for Carbon Dioxide Reduction. *Nat. Commun.* **2014**, *5*, No. 3242.
(34) Hatsukade, T.; Kuhl, K. P.; Cave, E. R.; Abram, D. N.; Jaramillo, T. F. Insights into the Electrocatalytic Reduction of CO_2 on Metallic Silver Surfaces. *Phys. Chem. Chem. Phys.* **2014**, *16*, 13814−13819.
(35) Xi, W.; Ma, R.; Wang, H.; Gao, Z.; Zhang, W.; Zhao, Y. Ultrathin Ag Nanowires Electrode for Electrochemical Syngas Production from Carbon Dioxide. *ACS Sustainable Chem. Eng.* **2018**, *6*, 7687−7694.
(36) Salvatore, D. A.; Weekes, D. M.; He, J.; Dettelbach, K. E.; Li, Y. C.; Mallouk, T. E.; Berlinguette, C. P. Electrolysis of Gaseous CO_2 to CO in a Flow Cell with a Bipolar Membrane. *ACS Energy Lett.* **2018**, *3*, 149−154.
(37) Gabardo, C. M.; Seifitokaldani, A.; Edwards, J. P.; Dinh, C. T.; Burdyny, T.; Kibria, M. G.; O'Brien, C. P.; Sargent, E. H.; Sinton, D. Combined High Alkalinity and Pressurization Enable Efficient CO_2 Electroreduction to CO. *Energy Environ. Sci.* **2018**, *11*, 2531−2539.
(38) Jhong, H. R. M.; Brushett, F. R.; Kenis, P. J. A. The Effects of Catalyst Layer Deposition Methodology on Electrode Performance. *Adv. Energy Mater.* **2013**, *3*, 589−599.
(39) Yano, H.; Shirai, F.; Nakayama, M.; Ogura, K. Electrochemical Reduction of CO_2 at Three-Phase (Gas | Liquid | Solid) and Two-Phase (Liquid | Solid) Interfaces on Ag Electrodes. *J. Electroanal. Chem.* **2002**, *533*, 113−118.
(40) Lu, X.; Leung, D. Y. C.; Wang, H.; Xuan, J. A High Performance Dual Electrolyte Microfluidic Reactor for the Utilization of CO_2. *Appl. Energy* **2017**, *194*, 549−559.
(41) Angulo, A.; van der Linde, P.; Gardeniers, H.; Modestino, M.; Fernández Rivas, D. Influence of Bubbles on the Energy Conversion Efficiency of Electrochemical Reactors. *Joule* **2020**, *4*, 555−579.
(42) Srikanth, S.; Singh, D.; Vanbroekhoven, K.; Pant, D.; Kumar, M.; Puri, S. K.; Ramakumar, S. S. V. Electro-Biocatalytic Conversion of Carbon Dioxide to Alcohols Using Gas Diffusion Electrode. *Bioresour. Technol.* **2018**, *265*, 45−51.
(43) Jiang, Y.; Su, M.; Zhang, Y.; Zhan, G.; Tao, Y.; Li, D. Bioelectrochemical Systems for Simultaneously Production of Methane and Acetate from Carbon Dioxide at Relatively High Rate. *Int. J. Hydrogen Energy* **2013**, *38*, 3497−3502.
(44) Loeppmann, S.; Breidenbach, A.; Spielvogel, S.; Dippold, M. A.; Blagodatskaya, E. Organic Nutrients Induced Coupled C- and P-Cycling Enzyme Activities During Microbial Growth in Forest Soils. *Front. For. Global Change* **2020**, *3*, No. 100.
(45) Rosso, L.; Lobry, J. R.; Bajard, S.; Flandrois, J. P. Convenient Model to Describe the Combined Effects of Temperature and PH on Microbial Growth. *Appl. Environ. Microbiol.* **1995**, *61*, 610−616.
(46) Clarke, K. G. *Bioprocess Engineering: An Introductory Engineering and Life Science Approach*; Elsevier, 2013.
(47) Jack, J.; Lo, J.; Donohue, B.; Maness, P.-C.; Jason Ren, Z. High Rate CO_2 Valorization to Organics via CO Mediated Silica Nanoparticle Enhanced Fermentation. *Appl. Energy* **2020**, *279*, No. 115725.
(48) Ooka, H.; Figueiredo, M. C.; Koper, M. T. M. Competition between Hydrogen Evolution and Carbon Dioxide Reduction on Copper Electrodes in Mildly Acidic Media. *Langmuir* **2017**, *33*, 9307−9313.
(49) Gaudreau, H.; Renard, N.; Champagne, C. P.; Van Horn, D. The Evaluation of Mixtures of Yeast and Potato Extracts in Growth Media for Biomass Production of Lactic Cultures. *Can. J. Microbiol.* **2002**, *48*, 626−634.
(50) Li, X.; Li, Z.; Zheng, J.; Shi, Z.; Li, L. Yeast Extract Promotes Phase Shift of Bio-Butanol Fermentation by Clostridium Acetobutylicum ATCC824 Using Cassava as Substrate. *Bioresour. Technol.* **2012**, *125*, 43−51.
(51) Hou, D.; Iddya, A.; Chen, X.; Wang, M.; Zhang, W.; Ding, Y.; Jassby, D.; Ren, Z. J. Nickel-Based Membrane Electrodes Enable High-Rate Electrochemical Ammonia Recovery. *Environ. Sci. Technol.* **2018**, *52*, 8930−8938.
(52) Wuttig, A.; Surendranath, Y. Impurity Ion Complexation Enhances Carbon Dioxide Reduction Catalysis. *ACS Catal.* **2015**, *5*, 4479−4484.

https://doi.org/10.1021/acssuschemeng.1c01150
ACS Sustainable Chem. Eng. 2021, 9, 6012−6022

(53) Xiu, Z. M.; Zhang, Q. B.; Puppala, H. L.; Colvin, V. L.; Alvarez, P. J. J. Negligible Particle-Specific Antibacterial Activity of Silver Nanoparticles. *Nano Lett.* **2012**, *12*, 4271−4275.

https://doi.org/10.1021/acssuschemeng.1c01150
ACS Sustainable Chem. Eng. 2021, 9, 6012−6022